

Adaptive Grids in the Context of Algebraic Stabilizations for Convection-Diffusion-Reaction Equations

Abhinav Jha ^{*}, Volker John [†], Petr Knobloch [‡]

Abstract

Three algebraically stabilized finite element schemes for discretizing convection-diffusion-reaction equations are studied on adaptively refined grids. These schemes are the algebraic flux correction (AFC) scheme with Kuzmin limiter, the AFC scheme with BJK limiter, and the recently proposed Monotone Upwind-type Algebraically Stabilized (MUAS) method. Both, conforming closure of the refined grids and grids with hanging vertices are considered. A non-standard algorithmic step becomes necessary before these schemes can be applied on grids with hanging vertices. The assessment of the schemes is performed with respect to the satisfaction of the global discrete maximum principle (DMP), the accuracy, e.g., smearing of layers, and the efficiency in solving the corresponding nonlinear problems.

Keywords: steady-state convection-diffusion-reaction equations; algebraically stabilized finite element methods; adaptive grid refinement; conforming closure; hanging vertices; discrete maximum principle (DMP)

AMS : 65N12, 65N30

1 Introduction

The physical behavior of scalar quantities, like temperature (energy) or concentrations, in fluids is modeled by scalar convection-diffusion-reaction equations. Let $\Omega \subset \mathbb{R}^d$, $d \in \{2, 3\}$, be a bounded domain with a Lipschitz-continuous boundary $\partial\Omega$. In this paper, we consider the steady-state equations, which are given, already in non-dimensional form, as follows:

$$\begin{aligned} -\varepsilon\Delta u + \mathbf{b} \cdot \nabla u + cu &= f \quad \text{in } \Omega \\ u &= u_b \quad \text{on } \Gamma_D, \\ \varepsilon\nabla u \cdot \mathbf{n} &= g \quad \text{on } \Gamma_N. \end{aligned} \tag{1}$$

Here, $\varepsilon > 0$ is the diffusion coefficient, $\mathbf{b} \in W^{1,\infty}(\Omega)^d$ is the convective field, $c \in L^\infty(\Omega)$ is the reaction field, $f \in L^2(\Omega)$ is the source or the sink term, $u_b \in H^{1/2}(\Gamma_D)$ and $g \in L^2(\Gamma_N)$ specify the boundary conditions, \mathbf{n} is the unit outward normal to $\partial\Omega$, $\Gamma_D \cup \Gamma_N = \partial\Omega$, $\Gamma_D \cap \Gamma_N = \emptyset$, Γ_D is the Dirichlet boundary and Γ_N is the Neumann boundary. Under appropriate assumptions on the data, it is well known that problem (1) possesses a unique weak solution.

In practice, the convective transport usually dominates the diffusive transport. One speaks of the convection-dominated regime, given if $\varepsilon \ll L\|\mathbf{b}\|_{L^\infty(\Omega)}$, where L is a characteristic length scale of the problem. Then, a characteristic feature of solutions of (1) are layers, which are thin regions with a steep gradient.

^{*}RWTH Aachen University, Applied and Computational Mathematics, Schinkelstraße 2, 52062, Aachen, Germany, Email: jha@acom.rwth-aachen.de

[†]Weierstrass Institute for Applied Analysis and Stochastics (WIAS), Mohrenstr. 39, 10117 Berlin, Germany and Freie Universität Berlin, Department of Mathematics and Computer Science, Arnimallee 6, 14195 Berlin, Germany, Email: john@wias-berlin.de

[‡]Department of Numerical Mathematics, Faculty of Mathematics and Physics, Charles University, Sokolovská 83, Praha 8, 18675, Czech Republic, Email: knobloch@karlin.mff.cuni.cz

In general, computational grids cannot resolve layers. It is well known that one has to apply so-called stabilized discretizations in this situation, e.g., see [27]. There are many proposals of such discretizations for convection-diffusion-reaction equations in the literature.

For appropriate data, the solution of (1) takes only certain physical values, e.g., concentrations are non-negative. The mathematical formulation of this physical feature is called maximum principle, see [11]. For numerical simulations in practice, it is often of utmost importance that also the discrete solution possesses only physically consistent values, i.e., it satisfies a discrete maximum principle (DMP). However, there are only very few among the stabilized discretizations with this property. The currently most promising class of methods seems to be the class of algebraically stabilized schemes.

Algebraically stabilized discretizations have been becoming quite popular for a couple of years. Their construction relies (mainly) on the algebraic system of equations from the Galerkin finite element discretization of (1) with conforming piecewise linear finite elements. Then, an algebraic stabilization term is introduced and certain coefficients (limiters) are computed that depend on the concrete discrete solution. Hence, these methods are nonlinear. The first comprehensive numerical analysis for the so-called algebraic flux correction (AFC) scheme with Kuzmin limiter, from [25], was presented in [4]. The AFC scheme with BJK limiter was proposed and analyzed in [5]. Recently, a new algebraically stabilized method was proposed in [20], which is called Monotone Upwind-type Algebraically Stabilized (MUAS) method. For all these methods, DMPs could be proved, sometimes under appropriate assumptions. For a detailed presentation of the methods and a discussion of the DMPs, we refer to Section 3.

Because of the presence of layers, where discrete solutions usually possess large errors, it is very attractive to use adaptively refined grids for the numerical solution of convection-diffusion-reaction equations. The control of adaptive grid refinement relies on an a posteriori error estimator or indicator. The first error estimator for the AFC schemes with Kuzmin and with BJK limiter has been proposed recently in [16]. On the basis of the error estimator or indicator, certain mesh cells are marked for refinement. Some of the common strategies to refine a grid can be found in [26, 3, 24]. The first step of refining a grid, i.e., the refinement of the marked cells, leads to the formation of hanging vertices. In the framework of discontinuous finite elements, the handling of grids with hanging vertices is rather easy to understand, see [1]. For continuous finite elements, the framework becomes more involved. A commonly used way around this issue is to use conforming closure or red-green refinements, see [3], but this approach leads to the deterioration of angles. Also, while using hexahedral mesh cells in 3d, the green completion leads to the formation of pyramids or prisms, which are not easy to handle by many finite element codes. Hence, using grids with hanging vertices is attractive from the geometric point of view, because one can perform a simple grid refinement.

This paper explores the behavior of the three above-mentioned algebraically stabilized methods in simulations on adaptive grids in two dimensions. An initial comparison of the AFC schemes was performed in [16], with the emphasis on studying the performance of two a posteriori error estimators in terms of their effectivity indices and their control of the adaptive refinement process. Concerning the MUAS method, some of its properties are illustrated numerically with simulations on uniform grids in [20]. In the current paper, first studies of this method on adaptively refined grids will be presented. The goal of the numerical studies consists in comparing the methods with respect to accuracy, to the satisfaction of the global DMP, and to efficiency in solving the nonlinear problems. A particular attention will be paid to the study of algebraic stabilizations on grids with hanging vertices. To the best of our knowledge, there is no such study in the literature so far. We could find the use of an algebraic stabilization on grids with hanging nodes only for the linear transport equation in [6]. From the algorithmic point of view, it will be shown that compared with the standard approach of modifying a linear system of equations for discretizations on grids with hanging nodes, an additional step becomes necessary for algebraically stabilized schemes, namely the transform to conforming ansatz functions. Such a step is not reported in [6].

The paper is organized as follows. Section 2 introduces concepts of triangulations, in particular with hanging vertices, and corresponding finite element spaces. The algebraically stabilized methods are described in Section 3. Some information concerning the implementation of these discretizations on grids with hanging vertices are provided in Section 4. The numerical studies are presented in Section 5. Section 6 summarizes the findings of this paper.

2 Triangulations and Finite Element Spaces

This section introduces notations and recalls concepts with respect to triangulations and finite element spaces. A special emphasis is paid to triangulations with hanging vertices. Some work concerning this topic can be found in [12], where results are provided for the lowest order Lagrange elements in the framework of multigrid methods. Recently, in [15] the theory has been extended for higher order Lagrange elements. Most of the definitions in this section follow standard texts, e. g., see [8, 7].

Let $\Omega \subset \mathbb{R}^d$, $d \in \{2, 3\}$, be a polygonal resp. polyhedral domain that is decomposed into simplices (i.e., triangles resp. tetrahedra). This decomposition is referred to as triangulation and is denoted by \mathcal{T}_h . As usual, it is assumed that the interiors of any two different elements of \mathcal{T}_h are disjoint and that $\bar{\Omega} = \cup_{K \in \mathcal{T}_h} K$. A triangulation \mathcal{T}_h of Ω is called conforming if, for any $K_1, K_2 \in \mathcal{T}_h$ with $K_1 \neq K_2$, the intersection $K_1 \cap K_2$ is either empty or a vertex or an edge or, in 3d, a face of both K_1 and K_2 . It is assumed that any edge or face lying on $\partial\Omega$ is a subset of either $\bar{\Gamma}_D$ or $\bar{\Gamma}_N$.

For a given triangulation \mathcal{T}_h , we denote by \mathcal{N}_h the set of all vertices, by \mathcal{E}_h the set of all edges, and by \mathcal{F}_h the set of all facets (i.e., all edges resp. faces). Thus, in 2d, it holds that $\mathcal{E}_h = \mathcal{F}_h$. The set of facets can be decomposed into $\mathcal{F}_h = \mathcal{F}_{h,\Omega} \cup \mathcal{F}_{h,D} \cup \mathcal{F}_{h,N}$, where $\mathcal{F}_{h,\Omega}$, $\mathcal{F}_{h,D}$, and $\mathcal{F}_{h,N}$ are the interior, Dirichlet, and Neumann facets, respectively. We denote the diameter of a mesh cell K by h_K and the diameter of an edge E and a facet F by h_E and h_F , respectively.

Definition 1 (Refinement, [12], Def. 3.3) *Let \mathcal{T}_1 and \mathcal{T}_2 be triangulations of Ω . Then, \mathcal{T}_2 is called a refinement of \mathcal{T}_1 if for all $K \in \mathcal{T}_1$ the set $\{K' \in \mathcal{T}_2 : K' \cap \text{int } K \neq \emptyset\}$ is a triangulation of K , where $\text{int } K$ is the interior of K .*

Definition 2 (Grid hierarchy, [12], Def. 3.4) *A family $\{\mathcal{T}_i\}_{i=0}^j$ is called a grid hierarchy on Ω if \mathcal{T}_0 is a conforming triangulation of Ω and if each \mathcal{T}_i , $i = 1, \dots, j$, is a refinement of \mathcal{T}_{i-1} .*

Definition 3 (Hanging vertex, [12], Def. 3.6) *Let \mathcal{T}_h be a triangulation of Ω . Then, a vertex $p \in \mathcal{N}_h$ is called a hanging vertex if there is an element $K \in \mathcal{T}_h$ with $p \in \partial K$ but p is not a vertex of K . The set of all hanging vertices is denoted by \mathcal{H}_h .*

In this work, we will consider first order Lagrange finite element spaces

$$S(\mathcal{T}_h) := \{v \in \mathcal{C}(\bar{\Omega}) : v|_K \in \mathbb{P}_1(K) \quad \forall K \in \mathcal{T}_h\}$$

consisting of continuous functions on $\bar{\Omega}$ such that the restrictions to all cells $K \in \mathcal{T}_h$ are polynomials of degree at most 1. It is well known that $S(\mathcal{T}_h) \subset H^1(\Omega)$. Degrees of freedom which determine functions from $S(\mathcal{T}_h)$ are values at vertices. Therefore, vertices are also called nodes. Due to the continuity requirement, values at hanging nodes depend on the values at non-hanging nodes as it is stated in the following lemma.

Lemma 4 ([12, Lemma 3.2]) *Let $\{\mathcal{T}_0, \dots, \mathcal{T}_j\}$ be a grid hierarchy on Ω . Let us denote $\mathcal{T}_h = \mathcal{T}_j$, i.e., the final refinement level. Then, for all $q \in \mathcal{H}_h$ there are coefficients a_{qp} with $p \in \mathcal{N}_h \setminus \mathcal{H}_h$ such that all $v \in S(\mathcal{T}_h)$ can be represented as*

$$v(q) = \sum_{p \in \mathcal{N}_h \setminus \mathcal{H}_h} a_{qp} v(p). \quad (2)$$

For conforming triangulations, a basis of $S(\mathcal{T}_h)$ is given by the well-known nodal basis functions. To construct basis functions of $S(\mathcal{T}_h)$ for a non-conforming triangulation, we first introduce non-conforming nodal basis functions that are generally not in $S(\mathcal{T}_h)$.

Definition 5 (Non-conforming nodal basis functions) *Let \mathcal{T}_h be a triangulation of Ω . Then, the non-conforming nodal basis function $\varphi_p^{\text{nc}} \in L^2(\Omega)$ associated with $p \in \mathcal{N}_h$ is defined as follows: For all $K \in \mathcal{T}_h$ there is a representative $\varphi_p^{\text{nc}}|_K = \mu_{p,K} \in \mathbb{P}_1(K)$ with $\mu_{p,K}(q) = \delta_{pq}$ for all vertices q of K .*

For a conforming mesh \mathcal{T}_h this definition reduces to $\varphi_p^{\text{nc}} \in S(\mathcal{T}_h)$ and $\varphi_p^{\text{nc}}(q) = \delta_{pq}$ for all $p, q \in \mathcal{N}_h$, i.e., the set $\{\varphi_p^{\text{nc}}\}_{p \in \mathcal{N}_h}$ is the conforming nodal basis of $S(\mathcal{T}_h)$. For a non-conforming triangulation, $S(\mathcal{T}_h)$ is in general only a subspace of the non-conforming finite element space

$$S^{\text{nc}}(\mathcal{T}_h) := \text{span} \{ \varphi_p^{\text{nc}} : p \in \mathcal{N}_h \}.$$

However, it is possible to construct a basis of $S(\mathcal{T}_h)$ from the non-conforming nodal basis of $S^{\text{nc}}(\mathcal{T}_h)$.

Theorem 6 ([12, Theorem 3.1]) *Let $\{\mathcal{T}_0, \dots, \mathcal{T}_j\}$ be a grid hierarchy on Ω . Let us denote $\mathcal{T}_h = \mathcal{T}_j$, i.e., the final refinement level. Then, a basis of $S(\mathcal{T}_h)$ is given by*

$$\left\{ \varphi_p = \varphi_p^{\text{nc}} + \sum_{q \in \mathcal{H}_h} a_{qp} \varphi_q^{\text{nc}} : p \in \mathcal{N}_h \setminus \mathcal{H}_h \right\},$$

where the coefficients a_{qp} are the same as in Lemma 4.

3 Algebraically Stabilized Schemes

As already mentioned, algebraic stabilizations are currently the most promising finite element discretizations for computing numerical solutions of steady-state convection-diffusion-reaction equations that satisfy DMPs. This section presents the methods that will be studied.

The first step of algebraically stabilized schemes consists in applying the standard Galerkin finite element method to the weak form of (1). Then, the discrete solution can be represented as a vector $U \in \mathbb{R}^N$, with the last $N - M$ components corresponding to the Dirichlet boundary conditions. The algebraic representation of the method is given by

$$AU = b,$$

where $A = (a_{ij})_{i,j=1}^N$ is the corresponding stiffness matrix and $b \in \mathbb{R}^N$ is the assembled right-hand side. In an algebraically stabilized method, an additional nonlinear stabilization term is added such that it takes the form

$$(A + B(U))U = b, \quad (3)$$

with $B(U) = (b_{ij}(U))_{i,j=1}^N$. For preserving conservation of the discrete solution, the stabilization has to be symmetric: $b_{ij}(U) = b_{ji}(U)$, $i, j = 1, \dots, M$.

3.1 AFC Scheme with Kuzmin Limiter

AFC schemes consider in the first step the Galerkin finite element discretization in the case that Neumann boundary conditions are applied, i.e., it is $M = N$. The stabilization term in (3) is of the form

$$b_{ij}(U) = (1 - \alpha_{ij}(U))d_{ij} \quad \forall i \neq j, \quad b_{ii}(U) = - \sum_{j \neq i} b_{ij}(U), \quad (4)$$

where $D = (d_{ij})_{i,j=1}^N$ is an artificial diffusion matrix with entries

$$d_{ij} = d_{ji} = - \max\{a_{ij}, 0, a_{ji}\} \quad \forall i \neq j, \quad d_{ii} = - \sum_{j \neq i} d_{ij}, \quad (5)$$

and $(\alpha_{ij}(U))_{i,j=1}^N$ is the limiter matrix with $0 \leq \alpha_{ij}(U) \leq 1$. After having computed the limiters, Dirichlet boundary conditions are imposed in the usual way.

In subregions where no layers appear, the standard Galerkin discretization can be applied. In this case, the corresponding limiters should be close to 1. In a vicinity of layers, a stabilization is necessary, which is achieved by using values of the limiter that are much smaller than 1.

The Kuzmin limiter, proposed in [25], is a monolithic upwind-type limiter and it is applicable to \mathbb{P}_1 and \mathbb{Q}_1 elements. For \mathbb{P}_1 elements, the existence of a solution is proved in [4]. For a real number a , denote $a^+ = \max\{a, 0\}$ and $a^- = \min\{a, 0\}$. Then, the limiters are computed as follows:

1. Compute

$$P_i^+ = \sum_{j=1, a_{ji} \leq a_{ij}}^N (d_{ij}(u_j - u_i))^+, \quad P_i^- = \sum_{j=1, a_{ji} \leq a_{ij}}^N (d_{ij}(u_j - u_i))^-.$$

2. Compute

$$Q_i^+ = - \sum_{j=1}^N (d_{ij}(u_j - u_i))^- , \quad Q_i^- = - \sum_{j=1}^N (d_{ij}(u_j - u_i))^+ .$$

3. Compute

$$R_i^+ = \min \left\{ 1, \frac{Q_i^+}{P_i^+} \right\}, \quad R_i^- = \min \left\{ 1, \frac{Q_i^-}{P_i^-} \right\}, \quad i = 1, \dots, M.$$

If P_i^+ or P_i^- is zero, one sets $R_i^+ = 1$ or $R_i^- = 1$, respectively. The values of R_i^+ and R_i^- are set to 1 for Dirichlet nodes as well.

4. If $a_{ji} \leq a_{ij}$, then set

$$\alpha_{ij} = \begin{cases} R_i^+ & \text{if } d_{ij}(u_j - u_i) > 0, \\ 1 & \text{if } d_{ij}(u_j - u_i) = 0, \\ R_i^- & \text{if } d_{ij}(u_j - u_i) < 0, \end{cases} \quad \alpha_{ji} := \alpha_{ij},$$

for $i, j = 1, \dots, N$. Note that the symmetry of the stabilization term follows from the symmetries of D and the limiters. For the Kuzmin limiter, the local DMP is satisfied if the off-diagonal entries of A possess a certain property, see [23] for details. It is also shown in this paper that this property and also the local DMP may be violated for certain types of triangulations, e.g., in two dimensions if the triangulation is not of Delaunay type

3.2 AFC Scheme with BJK Limiter

This method, proposed in [5], starts in the same way as the previous method and the stabilization term has the form (4). It was derived for \mathbb{P}_1 elements. For this method, the existence of a solution of the nonlinear problem and the satisfaction of a local and global DMP on arbitrary conforming simplicial grids can be proved. Moreover, it was shown in [5] that it is linearity preserving, i.e., the stabilization term vanishes for any vector that represents a linear function.

The computation of the limiter starts with a pre-processing step, compare [5, Eq. (2.4)]. Then, the computation proceeds as follows:

1. Compute

$$P_i^+ = \sum_{j=1}^N (d_{ij}(u_j - u_i))^+, \quad P_i^- = \sum_{j=1}^N (d_{ij}(u_j - u_i))^-.$$

2. Compute

$$Q_i^+ = q_i (u_i - u_i^{\max}), \quad Q_i^- = q_i (u_i - u_i^{\min}),$$

with

$$u_i^{\max} = \max_{j \in N_i \cup \{i\}} u_j, \quad u_i^{\min} = \min_{j \in N_i \cup \{i\}} u_j, \quad q_i = \sum_{j \in N_i} \gamma_i d_{ij},$$

where $N_i = \{j \in \{1, \dots, N\} \setminus \{i\} : a_{ij} \neq 0 \text{ or } a_{ji} > 0\}$ and γ_i is a positive constant which guarantees the linearity preservation, see Section 4 for details.

3. Compute

$$R_i^+ = \min \left\{ 1, \frac{Q_i^+}{P_i^+} \right\}, \quad R_i^- = \min \left\{ 1, \frac{Q_i^-}{P_i^-} \right\}, \quad i = 1, \dots, M.$$

If P_i^+ or P_i^- is zero, one sets $R_i^+ = 1$ or $R_i^- = 1$, respectively. The values for R_i^+ and R_i^- are set to 1 also for Dirichlet nodes.

4. Compute

$$\bar{\alpha}_{ij} = \begin{cases} R_i^+ & \text{if } d_{ij}(u_j - u_i) > 0, \\ 1 & \text{if } d_{ij}(u_j - u_i) = 0, \\ R_i^- & \text{if } d_{ij}(u_j - u_i) < 0, \end{cases} \quad i, j = 1, \dots, N.$$

Finally, one sets

$$\alpha_{ij} = \min \{ \bar{\alpha}_{ij}, \bar{\alpha}_{ji} \}, \quad i, j = 1, \dots, N.$$

Again, the symmetry of the stabilization term follows from the symmetries of D and of the limiters.

3.3 Monotone Upwind-type Algebraically Stabilized (MUAS) Method

The MUAS method was recently proposed and analyzed in [20], where the solvability of the nonlinear discrete problem and the satisfaction of local and global DMPs on arbitrary conforming simplicial grids are proved.

Also in this method, the matrix obtained for Neumann boundary conditions is considered in the first step. The stabilization term in (3) is given by

$$\begin{aligned} b_{ij}(U) &= -\max\{(1 - \alpha_{ij}(U))a_{ij}, 0, (1 - \alpha_{ji}(U))a_{ji}\}, \quad i, j = 1, \dots, N, \quad i \neq j, \\ b_{ii}(U) &= -\sum_{j=1, j \neq i}^N b_{ij}(U), \quad i = 1, \dots, N, \end{aligned}$$

which is clearly symmetric. The limiters $\alpha_{ij}(U)$ are computed as follows:

1. Compute

$$P_i^+ = \sum_{j=1, a_{ij} > 0}^N a_{ij}(u_i - u_j)^+, \quad P_i^- = \sum_{j=1, a_{ij} > 0}^N a_{ij}(u_i - u_j)^-.$$

2. Compute

$$Q_i^+ = \sum_{j=1}^N \max\{|a_{ij}|, a_{ji}\} (u_j - u_i)^+, \quad Q_i^- = \sum_{j=1}^N \max\{|a_{ij}|, a_{ji}\} (u_j - u_i)^-.$$

3. Compute

$$R_i^+ = \min \left\{ 1, \frac{Q_i^+}{P_i^+} \right\}, \quad R_i^- = \min \left\{ 1, \frac{Q_i^-}{P_i^-} \right\}, \quad i = 1, \dots, M.$$

If P_i^+ or P_i^- is zero, one sets $R_i^+ = 1$ or $R_i^- = 1$, respectively. The values of R_i^+ and R_i^- are set to 1 for Dirichlet nodes as well.

4. Define

$$\alpha_{ij} = \begin{cases} R_i^+ & \text{if } u_i > u_j, \\ 1 & \text{if } u_i = u_j, \\ R_i^- & \text{if } u_i < u_j, \end{cases} \quad i, j = 1, \dots, N.$$

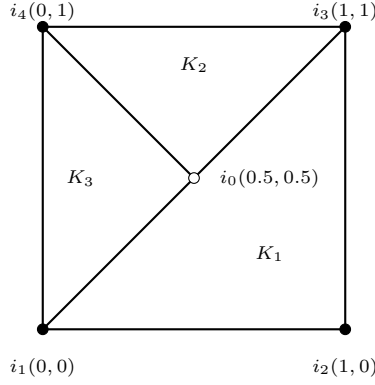


Figure 1: Patch considered in Examples 7 and 8.

4 Hanging Nodes and Algebraically Stabilized Schemes

For discretizations on grids with hanging nodes, first a linear system of equations for the non-conforming basis functions φ_p^{nc} , see Definition 5, is assembled. The next step consists in transforming this system to a system corresponding to conforming test functions φ_p , introduced in Theorem 6. Constraints are set for the values at the hanging nodes such that the finite element solution becomes continuous. An example will illustrate this approach.

Example 7 (System corresponding to non-conforming ansatz and conforming test functions) Consider a patch as defined in Figure 1. The non-conforming space $S^{\text{nc}}(\mathcal{T}_h)$ is spanned from the following basis functions:

$$\begin{aligned} \varphi_{i_0}^{\text{nc}}(x, y) &= \begin{cases} 0 & \text{in } K_1, \\ 2 - 2y & \text{in } K_2, \\ 2x & \text{in } K_3, \end{cases} & \varphi_{i_1}^{\text{nc}}(x, y) &= \begin{cases} 1 - x & \text{in } K_1, \\ 0 & \text{in } K_2, \\ 1 - x - y & \text{in } K_3, \end{cases} \\ \varphi_{i_2}^{\text{nc}}(x, y) &= \begin{cases} x - y & \text{in } K_1, \\ 0 & \text{in } K_2, \\ 0 & \text{in } K_3, \end{cases} & \varphi_{i_3}^{\text{nc}}(x, y) &= \begin{cases} y & \text{in } K_1, \\ x + y - 1 & \text{in } K_2, \\ 0 & \text{in } K_3, \end{cases} \\ \varphi_{i_4}^{\text{nc}}(x, y) &= \begin{cases} 0 & \text{in } K_1, \\ -x + y & \text{in } K_2, \\ -x + y & \text{in } K_3. \end{cases} \end{aligned}$$

The conforming space is $S(\mathcal{T}_h) = \text{span}\{\varphi_j \mid j \in \{i_1, \dots, i_4\}\}$, where the continuous basis functions are given by $\varphi_{i_j} = \varphi_{i_j}^{\text{nc}}$ for $j \in \{2, 4\}$ and

$$\varphi_{i_1} = \varphi_{i_1}^{\text{nc}} + \frac{1}{2}\varphi_{i_0}^{\text{nc}} = \begin{cases} 1 - x & \text{in } K_1, \\ 1 - y & \text{in } K_2, \\ 1 - y & \text{in } K_3, \end{cases} \quad \varphi_{i_3} = \varphi_{i_3}^{\text{nc}} + \frac{1}{2}\varphi_{i_0}^{\text{nc}} = \begin{cases} y & \text{in } K_1, \\ x & \text{in } K_2, \\ x & \text{in } K_3. \end{cases}$$

This means, the coefficients a_{qp} from Lemma 4 (with $q = 0$), given by $a_{qp} = \varphi_{i_p}^{\text{nc}}|_{K_1}$ evaluated at $(0.5, 0.5)$, are zero for $p \in \{2, 4\}$ and $1/2$ for $p \in \{1, 3\}$.

In standard finite element methods, the matrix and right-hand side are typically assembled cell-wise. This

approach can be performed also for the set of non-conforming basis functions $\varphi_{i_p}^{\text{nc}}$, $p = 0, \dots, 4$, leading to

$$\begin{pmatrix} a_{00} & a_{01} & a_{02} & a_{03} & a_{04} \\ a_{10} & a_{11} & a_{12} & a_{13} & a_{14} \\ a_{20} & a_{21} & a_{22} & a_{23} & a_{24} \\ a_{30} & a_{31} & a_{32} & a_{33} & a_{34} \\ a_{40} & a_{41} & a_{42} & a_{43} & a_{44} \end{pmatrix}, \quad \begin{pmatrix} b_0 \\ b_1 \\ b_2 \\ b_3 \\ b_4 \end{pmatrix}.$$

The p th equation of the corresponding linear system corresponds to the non-conforming test function $\varphi_{i_p}^{\text{nc}}$. In view of the above relations between conforming and non-conforming basis functions, equations corresponding to conforming test functions are obtained by adding $\frac{1}{2}$ of the 0th equation to the 1st and 3rd equations. To enforce continuity, the 0th equation is then replaced by the relation (2) with $q = 0$. This leads to the following matrix and right-hand side

$$\begin{pmatrix} 1 & -\frac{1}{2} & 0 & -\frac{1}{2} & 0 \\ a_{10} + \frac{a_{00}}{2} & a_{11} + \frac{a_{01}}{2} & a_{12} + \frac{a_{02}}{2} & a_{13} + \frac{a_{03}}{2} & a_{14} + \frac{a_{04}}{2} \\ a_{20} & a_{21} & a_{22} & a_{23} & a_{24} \\ a_{30} + \frac{a_{00}}{2} & a_{31} + \frac{a_{01}}{2} & a_{32} + \frac{a_{02}}{2} & a_{33} + \frac{a_{03}}{2} & a_{34} + \frac{a_{04}}{2} \\ a_{40} & a_{41} & a_{42} & a_{43} & a_{44} \end{pmatrix}, \quad \begin{pmatrix} 0 \\ b_1 + \frac{b_0}{2} \\ b_2 \\ b_3 + \frac{b_0}{2} \\ b_4 \end{pmatrix}. \quad (6)$$

□

Usually, a system with matrix and right-hand side from (6) is used for computing the numerical solution on grids with hanging nodes. But for algebraically stabilized schemes there is a new question: Which matrix should be used for computing the limiters? The proofs of the DMP use the assumption that the diagonal entries of the corresponding matrix are positive. However, this property cannot be guaranteed for the matrix from (6). In fact, numerical studies, which are not reported here for the sake of brevity, that used the limiters computed with this matrix led in several cases to unsatisfactory results, e.g., solutions obtained with the Kuzmin limiter showed spurious oscillation. Consequently, an additional step has to be performed for algebraically stabilized schemes, namely a transformation of the system to a form corresponding also to conforming ansatz functions. This means, the constraints for the hanging nodes are inserted in the other equations such that the corresponding matrix entries become zero.

Both steps, to the conforming test functions and to the conforming ansatz functions, extend the matrix stencil by few entries in rows that belong to test functions for non-hanging nodes which are located in a vicinity of hanging nodes.

Example 8 (System corresponding to conforming ansatz and test functions) Consider the matrix and right-hand side from (6). Inserting the equation for the finite element coefficient of $\varphi_{i_0}^{\text{nc}}$, which is the 0th equation, into the other equations, yields a matrix of the following form

$$\begin{pmatrix} 1 & -\frac{1}{2} & 0 & -\frac{1}{2} & 0 \\ 0 & a_{11} + \frac{a_{01}}{2} + \frac{a_{10}}{2} + \frac{a_{00}}{4} & a_{12} + \frac{a_{02}}{2} & a_{13} + \frac{a_{03}}{2} + \frac{a_{10}}{2} + \frac{a_{00}}{4} & a_{14} + \frac{a_{04}}{2} \\ 0 & a_{21} + \frac{a_{20}}{2} & a_{22} & a_{23} + \frac{a_{20}}{2} & a_{24} \\ 0 & a_{31} + \frac{a_{01}}{2} + \frac{a_{30}}{2} + \frac{a_{00}}{4} & a_{32} + \frac{a_{02}}{2} & a_{33} + \frac{a_{03}}{2} + \frac{a_{30}}{2} + \frac{a_{00}}{4} & a_{34} + \frac{a_{04}}{2} \\ 0 & a_{41} + \frac{a_{40}}{2} & a_{42} & a_{43} + \frac{a_{40}}{2} & a_{44} \end{pmatrix}. \quad (7)$$

□

The computation of the limiters is performed for the submatrix from (7) that corresponds to the rows and columns connected with non-hanging nodes. The Kuzmin and the MUAS limiter can be applied in a straightforward way. The set N_i in Step 2 of the BJK limiter is computed by exploring the entries of the i th row and taking all column indices of the corresponding sparsity pattern. Let $\Delta_i = \text{conv}\{x_j : j \in N_i\}$ be the convex hull of the nodes belonging to N_i . Then, the same definition as given in [5] can be used:

$$\gamma_i = \frac{\max_{x_j \in \partial\Delta_i} |x_i - x_j|}{\text{dist}(x_i, \partial\Delta_i)}, \quad i = 1, \dots, M.$$

5 Numerical Studies

This section presents numerical studies of algebraically stabilized schemes on adaptively refined grids. Both, grids with hanging nodes and grids with conforming closure will be considered and the results will be compared. Given a grid with hanging nodes that should be closed in a conforming way, then the closure might increase the largest angle or decrease the smallest angle of the triangles of the grid. The refinement with hanging nodes was performed such that there is not more than one hanging node per edge.

Using adaptively refined grids requires some criterion for controlling the local refinement. Usually, a posteriori error estimators or indicators are utilized. For the considered methods there is a residual-based a posteriori error estimator for the AFC schemes with Kuzmin and BJK limiter on conforming grids, which was proposed and analyzed in [16]. In this paper, actually two different techniques for calculating an upper bound for the error in the energy norm of solutions computed with AFC schemes on conforming grids are proposed. One of them uses a residual-based approach, which is referred to as AFC-energy technique, and the other one utilizes the SUPG estimator from [22], which is referred to as AFC-SUPG-energy technique. It was observed in [16] that the AFC-energy technique provides better results with respect to the refinement of the grids and hence we decided to use it as basis for our numerical studies.

Denote by $\|\cdot\|_{0,\omega}$ the norm of $L^2(\omega)$ for some set ω . In the AFC-energy technique, the error $u - u_h$ in the energy norm is bounded, i.e.,

$$\|u - u_h\|_a^2 \leq \eta^2 = \eta_1^2 + \eta_2^2 + \eta_3^2, \quad (8)$$

where $\|u\|_a^2 = \varepsilon \|\nabla u\|_{0,\Omega}^2 + \sigma_0 \|u\|_{0,\Omega}^2$, with $-(\nabla \cdot \mathbf{b}(\mathbf{x}))/2 + c(\mathbf{x}) \geq \sigma_0 > 0$ being assumed in Ω , and

$$\begin{aligned} \eta_1^2 &:= \sum_{K \in \mathcal{T}_h} \min \left\{ \frac{4C_I^2}{\sigma_0}, \frac{4C_I^2 h_K^2}{\varepsilon} \right\} \|R_K(u_h)\|_{0,K}^2, \\ \eta_2^2 &:= \sum_{F \in \mathcal{F}_h} \min \left\{ \frac{4C_F^2 h_F}{\varepsilon}, \frac{4C_F^2}{\sigma_0^{1/2} \varepsilon^{1/2}} \right\} \|R_F(u_h)\|_{0,F}^2, \\ \eta_3^2 &:= \sum_{E \in \mathcal{E}_h} \min \left\{ \frac{4\kappa_1 h_E^2}{\varepsilon}, \frac{4\kappa_2}{\sigma_0} \right\} (1 - \alpha_E)^2 |d_E|^{2-d} h_E^{1-d} \|\nabla u_h \cdot \mathbf{t}_E\|_{0,E}^2, \end{aligned}$$

u_h is the solution of the algebraically stabilized scheme, $\alpha_E = \alpha_{ij}$ and $d_E = d_{ij}$ for an edge E with endpoints x_i, x_j , \mathbf{t}_E is the unit tangent vector along the edge E , $R_K(u_h)$ and $R_F(u_h)$ stand for the residuals on mesh cell K and on the facet F given by

$$\begin{aligned} R_K(u_h) &:= (f + \varepsilon \Delta u_h - \mathbf{b} \cdot \nabla u_h - c u_h)|_K, \\ R_F(u_h) &:= \begin{cases} -\varepsilon [\![\nabla u_h \cdot \mathbf{n}_F]\!]_F & \text{if } F \in \mathcal{F}_{h,\Omega}, \\ g - \varepsilon (\nabla u_h \cdot \mathbf{n}_F) & \text{if } F \in \mathcal{F}_{h,N}, \\ 0 & \text{if } F \in \mathcal{F}_{h,D}, \end{cases} \end{aligned}$$

\mathbf{n}_F is the unit normal on facet F , and $[\![\cdot]\!]_F$ denotes the jump across F .

The constants C_I and C_F appear from the interpolation and facet estimates and were set to unity in the simulations. The constants κ_1 and κ_2 are given by

$$\kappa_1 = C C_{\text{edge,max}} \left(1 + (1 + C_I)^2\right), \quad \kappa_2 = C C_{\text{inv}}^2 C_{\text{edge,max}} \left(1 + (1 + C_I)^2\right),$$

where C is a general constant independent of h , C_{inv} is an inverse inequality constant, and $C_{\text{edge,max}}$ is a computable constant given by [16, Remark 9]. Likewise as the other constants, C and C_{inv} were set to unity in our simulations. In [16], the error estimator η was applied to the two above-described AFC schemes on conforming grids.

Remark 9 The expression η from (8) can be computed also for the MUAS method and for all methods on grids with hanging nodes. Then, it is just an error indicator, i.e., there is no analysis. In practice, often

error indicators are used for controlling the adaptive grid refinement, like the popular gradient indicator. In preliminary studies, we could observe that for the AFC methods, the use of η on grids with hanging nodes led to a quite similar adaptive refinement process as for grids with conforming closure, i.e., the refinement starts at the strongest singularities (exponential layers) and regions with weaker singularities (parabolic layers) are refined somewhat later. For this reason, we applied η also for the AFC methods on grids with hanging nodes. In contrast, we detected that applying η for the MUAS method results in a simultaneous refinement in all regions with singularities and considerably different adaptive grids compared with the AFC methods. This situation made it difficult to compare the computational results. Neglecting the term η_3 for the MUAS method, which results in a standard residual-based error indicator, led to a similar behavior of the adaptive grid refinement process as for the AFC schemes. For this reason, the adaptive grid refinement for the MUAS method was controlled on all grids with $(\eta_1^2 + \eta_2^2)^{1/2}$. \square

A grid with conforming closure contains regularly refined cells and closure cells. Both types might be marked for refinement by the error indicator. In the first step of the refinement process, parents of closure cells are marked for refinement if one of its children is marked for refinement. Note that parents of closure cells are regularly refined cells on a coarser grid. Then, all closure cells are removed and all marked cells are refined regularly. Finally, the refined grid is closed. In the case of grids with hanging nodes, all marked cells are refined regularly. Then, a procedure is applied that refines all cells regularly that have an edge with more than one hanging node, until such cells are not contained any longer in the grid. The adaptive refinement process for the first two examples was stopped after the first adaptively refined grid where the number of degrees of freedom ($\#\text{dof}$) was $\gtrsim 2.5 \times 10^5$. The given numbers $\#\text{dof}$ contain always the hanging and the Dirichlet nodes.

Remark 10 *Comparative studies for the solution of the nonlinear problem arising in the AFC schemes were performed in [18, 17]. It was found that the simplest fixed point iteration scheme was the most efficient one. A brief description of this scheme is as follows. The matrix form of the algebraic stabilization given in (3) is reformulated as*

$$(A + D)U = b + (D - B(U))U,$$

with the artificial diffusion matrix D from (5). The matrix on the left-hand side is by construction an M -matrix. Then, a fixed point iteration of the form

$$(A + D)\tilde{U}^\mu = b + (D - B(U^\mu))U^\mu, \quad U^{\mu+1} = \omega\tilde{U}^\mu + (1 - \omega)U^\mu, \quad (9)$$

is applied, where μ denotes the μ^{th} iterative step and $\omega \in \mathbb{R}^+$ is a damping parameter, which is chosen dynamically. Using a sparse direct solver for the linear systems of equations in (9) exploits that the matrix on the left-hand side does not change during the iteration and hence its factorization needs to be computed only once. Also for iterative solvers, method (9) is well suited, because they usually converge quickly since the matrix is an M -matrix, compare [17]. A detailed description of this scheme, in particular of the dynamic damping procedure, can be found in [17], where it is referred to as ‘fixed-point right-hand side’. The nonlinear loops were stopped if 10,000 iteration steps were reached or if $\mathbf{res} \leq \varepsilon_{\text{thresh}}\sqrt{\#\text{dof}}$, where \mathbf{res} is the Euclidean norm of the residual vector and $\varepsilon_{\text{thresh}}$ is the stopping threshold. If not mentioned otherwise, then $\varepsilon_{\text{thresh}} = 10^{-10}$. \square

All schemes were used with \mathbb{P}_1 finite elements. The matrices were assembled exactly and the arising systems of linear equations were solved using the sparse direct solver UMFPACK, [9]. All simulations were performed with the in-house code PARMOON, [28, 10].

The numerical results will be compared on the basis of the satisfaction of the global DMP, the accuracy of solutions, e.g., measured by sharpness of layers, and efficiency, measured by the number of iterations and rejections for the solver of the nonlinear problem. After having rejected a step, the damping factor is decreased, but this step is computationally as expensive as an accepted step.

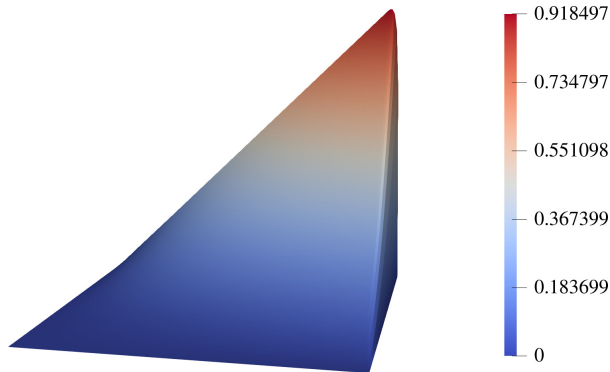


Figure 2: Example 5.1: Solution computed with AFC scheme and Kuzmin limiter, level 7 with uniform refinement.

5.1 Solution Becoming Locally Diffusion-Dominated under Adaptive Grid Refinement

This example, presented in [21], is given in $\Omega = (0, 1)^2$ with $\mathbf{b} = (2, 3)^T$, $c = 1$, and $\partial\Omega = \Gamma_D$. The solution

$$u(x, y) = xy^2 - y^2 \exp\left(\frac{2(x-1)}{\varepsilon}\right) - x \exp\left(\frac{3(y-1)}{\varepsilon}\right) + \exp\left(\frac{2(x-1) + 3(y-1)}{\varepsilon}\right),$$

defines the right-hand side f and the Dirichlet boundary condition u_b . It possesses boundary layers at $x = 1$ and $y = 1$, see Figure 2. We consider the case $\varepsilon = 10^{-2}$, i.e., the discrete problem is convection-dominated on coarse grids (the layers are not resolved) and it becomes diffusion-dominated on finer grids.

The initial mesh (level 0) was defined by dividing the domain into two triangles by joining the points $(0, 0)$ and $(1, 1)$. The simulations were started with the level 2 grid obtained by uniform refinement (i.e., $\#\text{dof} = 25$) and initially uniform refinement was applied until level 5 (i.e., $\#\text{dof} = 1089$). After that, adaptive refinement was performed.

Since the solution is known, errors of the discrete approximations computed with the algebraically stabilized schemes can be computed. Figure 3 presents the errors in the $L^2(\Omega)$ norm and in the $L^2(\Omega)$ norm of the gradient. It can be seen that the solutions computed with the AFC scheme with BJK limiter and with the MUAS scheme are likewise accurate. On both types of grids, the optimal convergence order of the error in the $L^2(\Omega)$ norm of the gradient can be seen. It has to be noted that the error estimator is for the error in the energy norm, which is dominated here by the $L^2(\Omega)$ error of the gradient, and not for the $L^2(\Omega)$ norm, such that the adaptive grids might not be always suitable for an optimal error convergence in the $L^2(\Omega)$ norm. The solutions obtained with the AFC scheme and Kuzmin limiter seem not to converge on grids with conforming closure and they converge slower on grids with hanging nodes. This behavior on conforming grids was already observed for a similar example in [16]. In fact, the analysis from [4] predicts that convergence can be expected for this method in the diffusion-dominated case only if the grid satisfies certain conditions, e.g., if the grid is Delaunay.

Figure 4 presents results concerning the efficiency of the methods. It can be observed that the AFC scheme with Kuzmin limiter needs usually the smallest number of iterations and the AFC scheme with BJK limiter often the largest number. But altogether, no difficulties arose for solving the nonlinear problems.

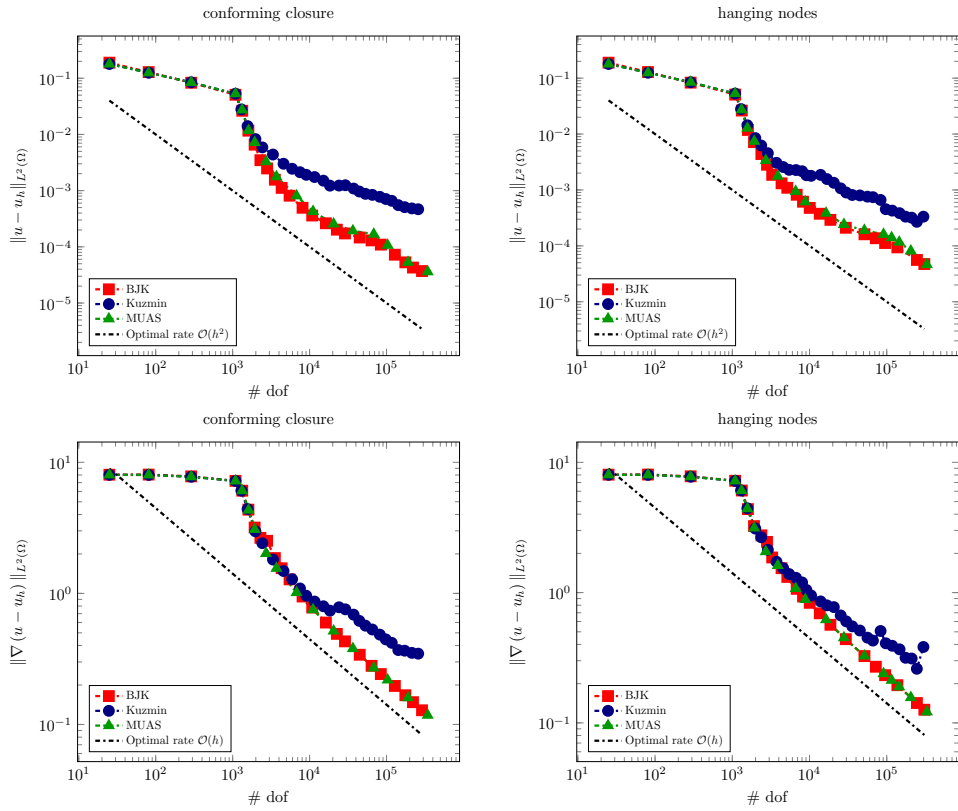


Figure 3: Example 5.1: $L^2(\Omega)$ error (top) and $L^2(\Omega)$ error of the gradient (bottom); grids with conforming closure (left) and grids with hanging nodes (right).

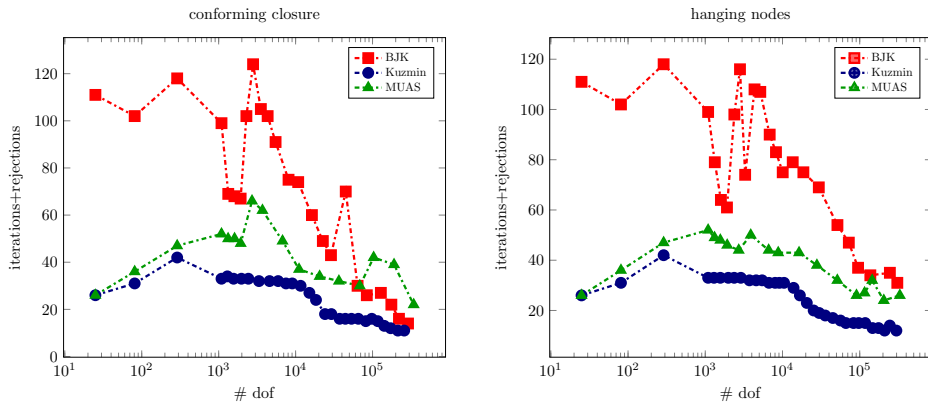


Figure 4: Example 5.1: Number of iterations and rejections on grids with conforming closure (left) and on grids with hanging nodes (right).

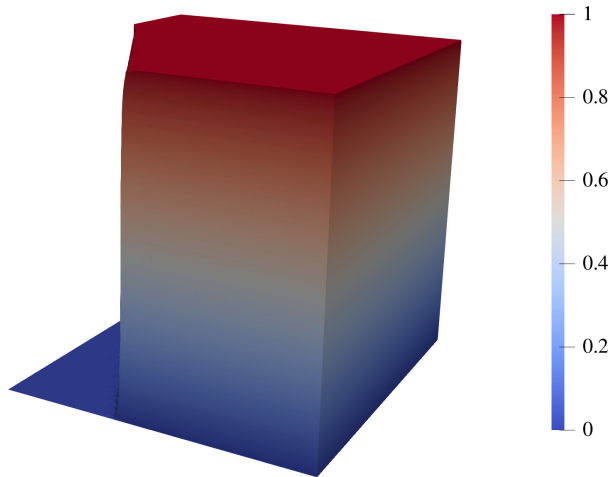


Figure 5: Example 5.2: Solution to the interior and boundary layer example, computed with the BJK limiter, level 9.

5.2 A Convection-Dominated Problem with Interior and Boundary Layers

This standard example was proposed in [14]. It is given in $\Omega = (0, 1)^2$ with $\mathbf{b} = (\cos(-\pi/3), \sin(-\pi/3))^T$, $c = f = 0$, and the Dirichlet boundary condition

$$u_b = \begin{cases} 1 & (y = 1 \wedge x > 0) \text{ or } (x = 0 \wedge y > 0.7), \\ 0 & \text{else.} \end{cases}$$

Here, the convection-dominated case $\varepsilon = 10^{-6}$ is considered. The solution exhibits an interior layer in the direction of the convection starting from the jump of the boundary condition at the left boundary and two exponential layers at the right and the lower boundary, see Figure 5. An analytic solution to this problem is not available, but the solution satisfies the global maximum principle, i.e., $u \in [0, 1]$. In the numerical studies, the satisfaction of the global DMP, the accuracy by considering the width of the interior layer along a cut line, and the efficiency will be studied. In addition, the impact of relaxing the stopping criterion of the iteration on the quantities of interest will be investigated.

The initial grid (level 0) was constructed by dividing the unit square with the diagonal from $(0, 1)$ to $(1, 0)$, as advised in [19]. The simulations were started on level 2 and uniform refinement was performed until level 5.

The satisfaction of the global DMP is studied by evaluating the quantity

$$\text{osc}_{\max}(u_h) := \max_{(x,y) \in \bar{\Omega}} u_h(x,y) - 1 - \min_{(x,y) \in \bar{\Omega}} u_h(x,y). \quad (10)$$

It turned out that these values were for all schemes and all grids at most of the order of round-off errors. Hence, the corresponding numerical solutions satisfy the global DMP.

To check the thickness of the interior layer, we follow the idea described in [19, Eq. (48)] and define

$$\text{smear}_{\text{int}} = x_2 - x_1, \quad (11)$$

where x_1 is the x -coordinate on the cut line $(x, 0.25)$ with $u_h(x_1, 0.25) = 0.1$ and x_2 is the x -coordinate with $u_h(x_2, 0.25) = 0.9$. The cut line was discretized with 100,000 equidistant intervals, where the discrete solutions were evaluated at the nodes. Then, the values for x_1 and x_2 were computed by linear interpolation. The results, presented in Figure 6, show that there are only minor differences between the solutions obtained

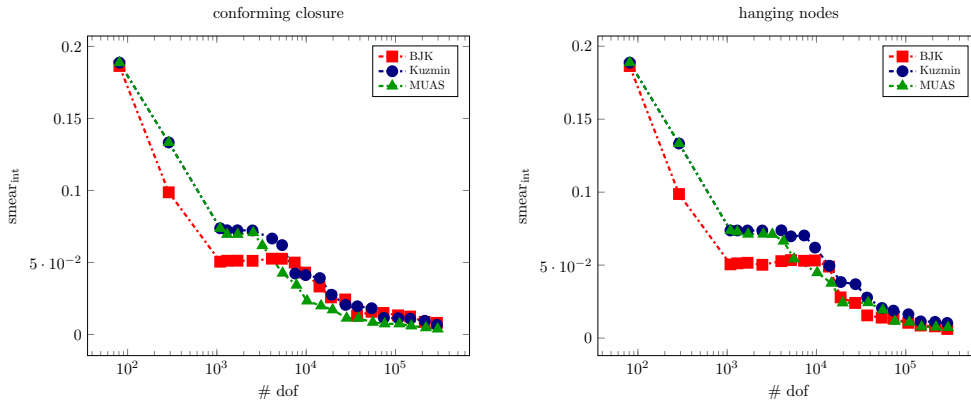


Figure 6: Example 5.2: Thickness of interior layer, $\text{smear}_{\text{int}}$.

with the different methods. On grids with hanging nodes, the AFC method with BJK limiter and the MUAS method computed usually a little bit sharper layers than the AFC method with Kuzmin limiter.

Figure 7 presents the number of iterations and rejections. It can be observed that the AFC method with BJK limiter sometimes stopped because the maximal number was reached, in particular on fine grids. The other two methods needed usually a similar and much smaller number of iterations. The rationale for choosing the hard stopping criterion with $\varepsilon_{\text{thresh}} = 10^{-10}$ is that analytic results, like the satisfaction of DMPs, can be proved only for the solution of the nonlinear discrete problem and thus an accurate solution seems to be advisable.

The number of iterations and rejections for the weaker stopping criteria with $\varepsilon_{\text{thresh}} = 10^{-6}$ and $\varepsilon_{\text{thresh}} = 10^{-8}$ are depicted also in Figure 7. It can be seen that in all situations the stopping criterion with respect to the residual could be satisfied now. The AFC scheme with Kuzmin limiter and the MUAS method require generally notably less iterations than the AFC scheme with BJK limiter.

Figure 8 provides information on the impact of the weaker stopping criteria on the satisfaction of the global DMP. Only for the weakest stopping criterion $\varepsilon_{\text{thresh}} = 10^{-6}$ and on fine grids there are notable spurious oscillations.

Concerning the width of the interior layer, we usually could not observe visible differences between the results from Figure 6 and the results for $\varepsilon_{\text{thresh}} = 10^{-8}$. Often, also the layer width of the solutions computed with $\varepsilon_{\text{thresh}} = 10^{-6}$ is similar. Only on very fine grids, we could see more smearing with this stopping criterion. For the sake of brevity, the results with respect to the layer width are not presented in detail.

Remark 11 *Continuing the adaptive refinement in this example creates very small mesh cells. We could observe that the sparse direct solver failed, giving `nan`, if cells with a diameter of around 10^{-6} occurred. In contrast, a standard iterative solver, GMRES with SSOR preconditioner, still worked well in this situation.* \square

5.3 Hemker Problem

The Hemker problem is a standard benchmark problem defined in [13]. The domain is given by $\Omega = \{(-3, 9) \times (-3, 3)\} \setminus \{(x, y) : x^2 + y^2 \leq 1\}$, the convection field by $\mathbf{b} = (1, 0)^T$, and the reaction field and right-hand side in Eq. (1) vanish: $c = f = 0$. Dirichlet boundary conditions are set at $x = -3$, with $u_b = 0$ and at the circular boundary with $u_b = 1$. On all other boundaries, homogeneous Neumann conditions are prescribed. This problem was studied comprehensively for $\varepsilon = 10^{-4}$ in [2] and reference values are available for some quantities of interest. This diffusion parameter was used also in our studies, see Figure 9 for an illustration of the solution, which takes values in $[0, 1]$.

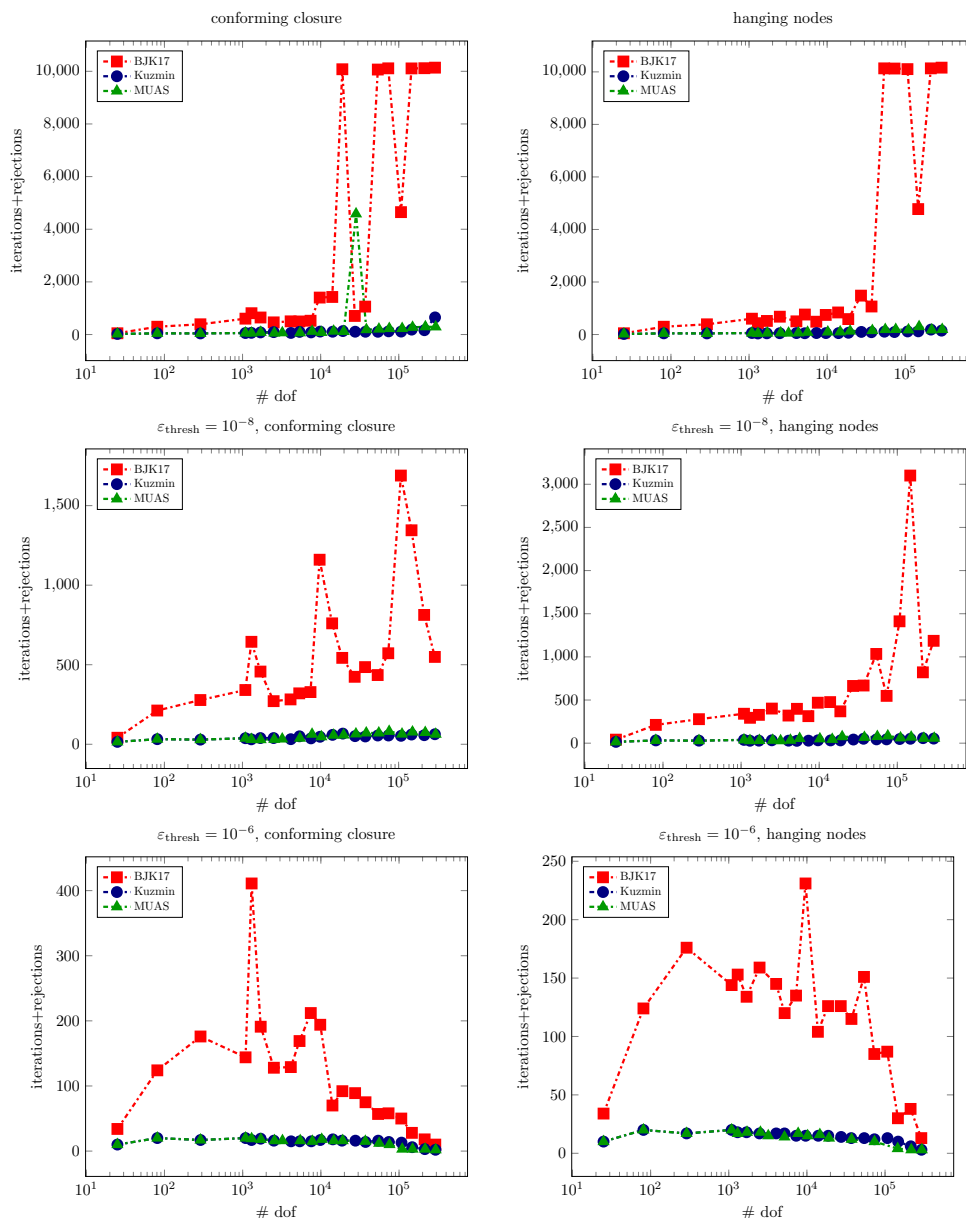


Figure 7: Example 5.2 Number of iterations and rejections on grids with conforming closure (left) and on grids with hanging nodes (right), $\epsilon_{\text{thresh}} = 10^{-10}$ (top), $\epsilon_{\text{thresh}} = 10^{-8}$ (middle), $\epsilon_{\text{thresh}} = 10^{-6}$ (bottom).

Figure 9 presents the initial grid with $\# \text{dof} = 151$. The adaptive refinement was started after having computed the solution on the initial grid. It was stopped when $\# \text{dof} \gtrsim 5 \times 10^5$. During refinement, the approximation of the circular boundary was improved. Based on the experience from the previous example, the threshold for stopping the iterative solution of the nonlinear problem was set to be $\epsilon_{\text{thresh}} = 10^{-8}$.

The satisfaction of the global DMP was measured again by $\text{osc}_{\max}(u_h)$ defined in (10). As in the previous example, for the AFC scheme with BJK limiter and the MUAS method, only unphysical values of the order of the stopping criterion for solving the nonlinear problems could be observed. Hence, these methods satisfy the global DMP. In contrast, there are small but notable spurious oscillations for the AFC scheme with

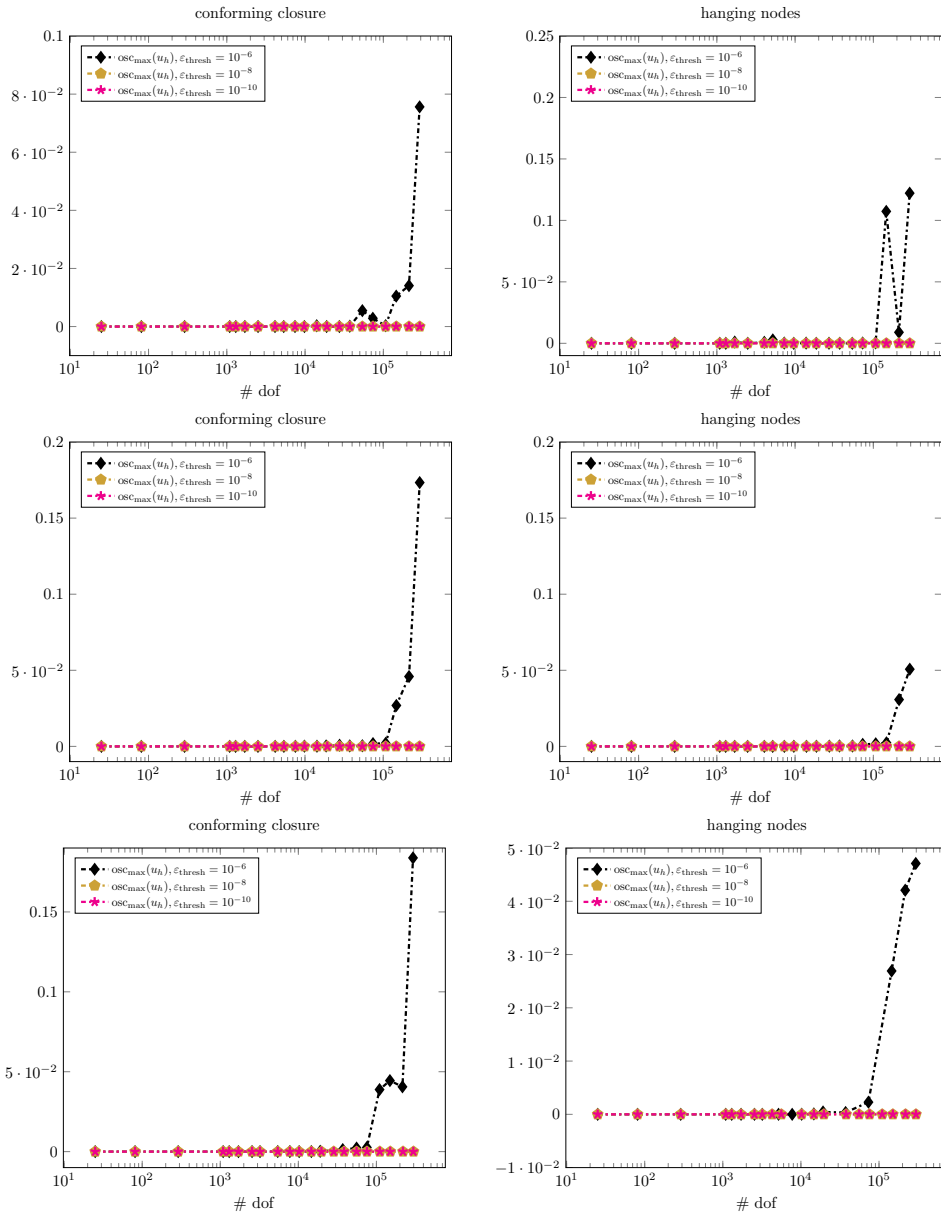


Figure 8: Example 5.2: Dependency of the spurious oscillations on the stopping criterion in the solver for the nonlinear problem: AFC scheme with BJK limiter (top), with Kuzmin limiter (middle), and MUAS method (bottom).

Kuzmin limiter on fine conforming grids, compare Figure 10. We think that the reason is the appearance of non-Delaunay closure cells in combination with the fact that the discrete problem becomes locally diffusion-dominated in strongly refined regions.

For assessing the accuracy of the solutions in [2], the width of the internal layer at $y = 1$ on the cut line at $x = 4$ was considered. The definition of the layer width is similar like for the quantity $\text{smear}_{\text{int}}$ from (11). In [2], the reference value 0.0723 is provided. The results obtained with the considered schemes are presented in Figure 11. In general, the sharpest layer was computed with AFC scheme with BJK limiter.

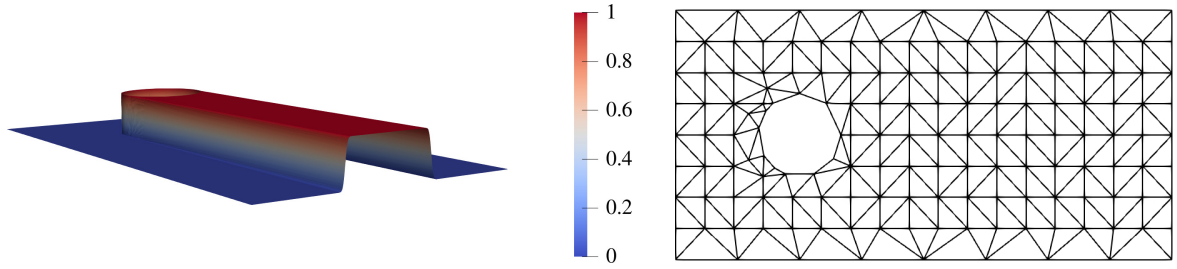


Figure 9: Example 5.3: Solution for $\varepsilon = 10^{-4}$ (left), computed with the BJK limiter, level 6; initial grid (right), level 0.

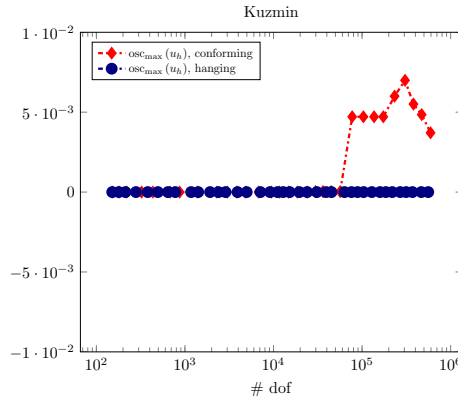


Figure 10: Example 5.3: Spurious oscillations for different grids with conforming closure and hanging nodes for the AFC scheme with Kuzmin limiter. There are no spurious oscillations for the solutions computed with the two other schemes.

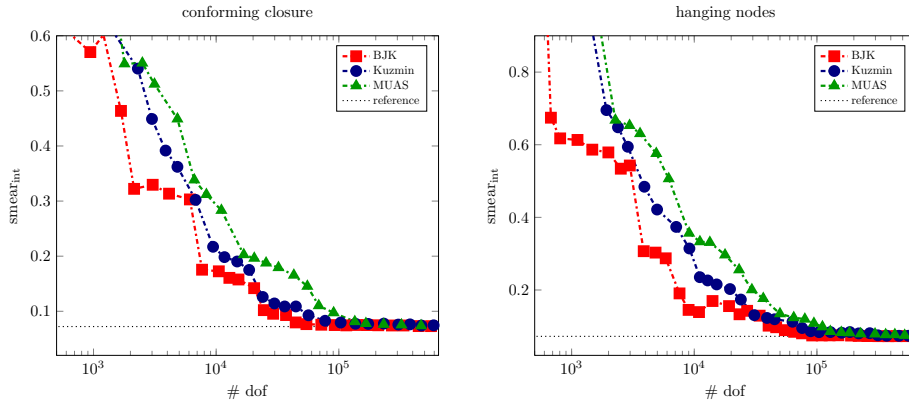


Figure 11: Example 5.3: Thickness of the internal layer at $x = 4$, $\text{smear}_{\text{int}}$.

On sufficiently fine grids, the results for all methods are very close to the reference value. Up to around 100,000 #dof, the results for the MUAS method are notably less accurate than for the other two methods. The reason is that the adaptive grid refinement occurred for this method in a somewhat different way, see Figure 12 for a representative example. For the AFC methods, the region of this cut line is already much stronger refined. This situation shows that there is the need of an improved mechanism for controlling the

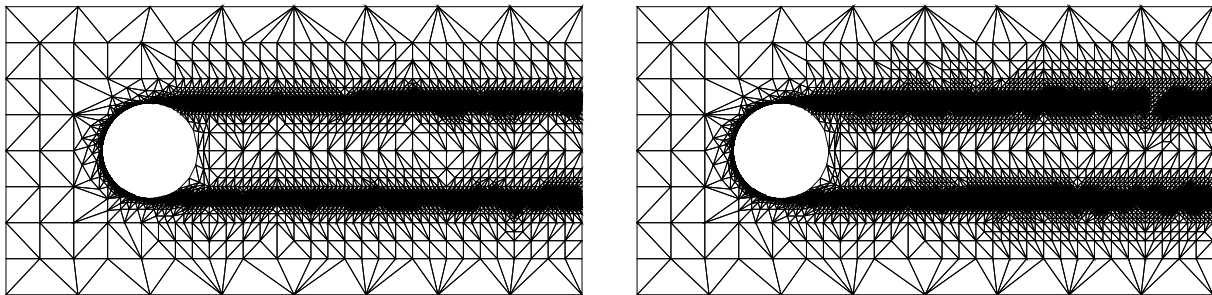


Figure 12: Example 5.3: Adaptively refined conforming grids with $\approx 25,000$ #dof, left with AFC method and Kuzmin limiter, right with MUAS method.

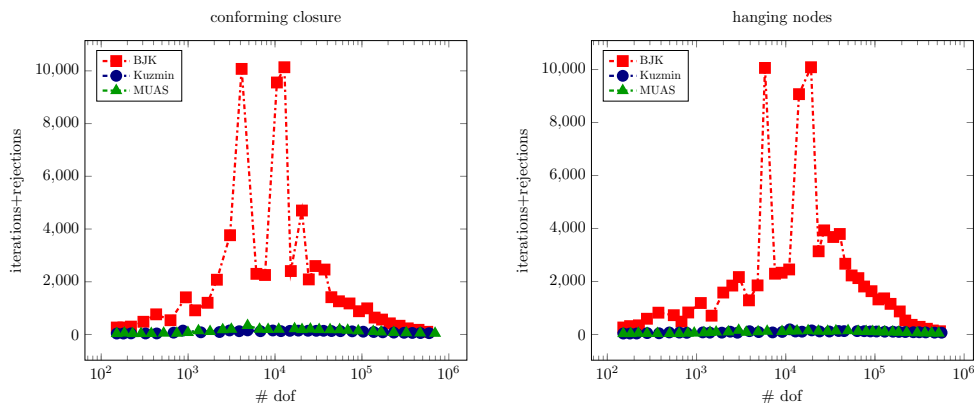


Figure 13: Example 5.3: Number of iterations and rejections.

adaptive grid refinement for the MUAS method, i.e., the need of developing an a posteriori error estimator.

Concerning the efficiency, the situation is similar as in Example 5.2. The simulations with the AFC scheme with Kuzmin limiter and the MUAS method needed generally a similar number of iterations, see Figure 13. They were often considerably more efficient than the simulations with the AFC scheme with BJK limiter.

5.4 Summary of the Numerical Studies

Here, the most important findings of the numerical studies are summarized.

- The global DMP was satisfied for all methods on all grids with hanging nodes. On grids with conforming closure, it was always satisfied for the AFC scheme with BJK limiter and the MUAS method.
- The AFC method with Kuzmin limiter did not always satisfy the DMP on conforming grids with locally very small mesh cells, where the discrete problem is locally diffusion-dominated.
- The AFC scheme with BJK limiter and the MUAS method converge if the discrete solution becomes (locally) diffusion-dominated, both on adaptive grids with conforming closure and with hanging nodes.
- If the discrete solution becomes (locally) diffusion-dominated, then the AFC method with Kuzmin limiter does not convergence on adaptively refined grids with conforming closure.
- The nonlinear problems could be solved often most efficiently for the AFC scheme with Kuzmin limiter and the MUAS method.

6 Summary

This paper studied the behavior of algebraic stabilizations for discretizing steady-state convection-diffusion-reaction equations in simulations on adaptively refined grids, both with conforming closure and with hanging nodes. The AFC scheme with BJK limiter and the MUAS method satisfied always the global DMP. It could be demonstrated that the failure of the AFC method with Kuzmin limiter to satisfy the DMP on some grids with conforming closure could be removed by using grids with hanging nodes. The crucial algorithmic component for a successful application of algebraically stabilized schemes on grids with hanging nodes is that the linear system of equations is transformed to conforming test and conforming ansatz functions for computing the limiters. In summary, taking all the aspects of accuracy, satisfaction of the global DMP, and efficiency into account, the MUAS method seems to be the most promising of the three approaches studied in this paper.

Acknowledgement

The work of Petr Knobloch has been supported through the grant No. 20-01074S of the Czech Science Foundation.

References

- [1] M. AINSWORTH AND R. RANKIN, *Fully computable error bounds for discontinuous galerkin finite element approximations on meshes with an arbitrary number of levels of hanging nodes*, SIAM Journal on Numerical Analysis, 47 (2010), pp. 4112–4141, <https://doi.org/10.1137/080725945>.
- [2] M. AUGUSTIN, A. CAIAZZO, A. FIEBACH, J. FUHRMANN, V. JOHN, A. LINKE, AND R. UMLA, *An assessment of discretizations for convection-dominated convection-diffusion equations*, Computer Methods in Applied Mechanics and Engineering, 200 (2011), pp. 3395–3409, <https://doi.org/10.1016/j.cma.2011.08.012>.
- [3] R. E. BANK, A. H. SHERMAN, AND A. WEISER, *Refinement algorithms and data structures for regular local mesh refinement*, in Scientific computing (Montreal, Que., 1982), IMACS Trans. Sci. Comput., I, IMACS, New Brunswick, NJ, 1983, pp. 3–17.
- [4] G. R. BARRENECHEA, V. JOHN, AND P. KNOBLOCH, *Analysis of algebraic flux correction schemes*, SIAM Journal on Numerical Analysis, 54 (2016), pp. 2427–2451, <https://doi.org/10.1137/15m1018216>.
- [5] G. R. BARRENECHEA, V. JOHN, AND P. KNOBLOCH, *An algebraic flux correction scheme satisfying the discrete maximum principle and linearity preservation on general meshes*, Mathematical Models and Methods in Applied Sciences, 27 (2017), pp. 525–548, <https://doi.org/10.1142/s0218202517500087>.
- [6] M. BITTL AND D. KUZMIN, *An hp-adaptive flux-corrected transport algorithm for continuous finite elements*, Computing, 95 (2013), pp. 27–48, <https://doi.org/10.1007/s00607-012-0223-y>.
- [7] S. C. BRENNER AND L. R. SCOTT, *The Mathematical Theory of Finite Element Methods*, Springer New York, 2008, <https://doi.org/10.1007/978-0-387-75934-0>.
- [8] P. G. CIARLET, *The finite element method for elliptic problems*, North-Holland Publishing Co., Amsterdam-New York-Oxford, 1978. Studies in Mathematics and its Applications, Vol. 4.
- [9] T. A. DAVIS, *Algorithm 832*, ACM Transactions on Mathematical Software, 30 (2004), pp. 196–199, <https://doi.org/10.1145/992200.992206>.

- [10] S. GANESAN, V. JOHN, G. MATTHIES, R. MEESALA, A. SHAMIM, AND U. WILBRANDT, *An object oriented parallel finite element scheme for computations of PDEs: Design and implementation*, in 2016 IEEE 23rd International Conference on High Performance Computing Workshops (HiPCW), IEEE, Dec. 2016, <https://doi.org/10.1109/hipcw.2016.023>.
- [11] D. GILBARG AND N. S. TRUDINGER, *Elliptic Partial Differential Equations of Second Order*, Springer Berlin Heidelberg, 2001, <https://doi.org/10.1007/978-3-642-61798-0>.
- [12] C. GRÄSER, *Convex minimization and phase field models*, PhD thesis, Freie Universität, Berlin, 2011.
- [13] P. HEMKER, *A singularly perturbed model problem for numerical computation*, Journal of Computational and Applied Mathematics, 76 (1996), pp. 277–285, [https://doi.org/10.1016/s0377-0427\(96\)00113-6](https://doi.org/10.1016/s0377-0427(96)00113-6).
- [14] T. J. HUGHES, M. MALLETT, AND M. AKIRA, *A new finite element formulation for computational fluid dynamics: II. beyond SUPG*, Computer Methods in Applied Mechanics and Engineering, 54 (1986), pp. 341–355, [https://doi.org/10.1016/0045-7825\(86\)90110-6](https://doi.org/10.1016/0045-7825(86)90110-6).
- [15] A. JHA, *Hanging nodes for higher-order lagrange finite elements*, Examples and Counterexamples, 1 (2021), p. 100025, <https://doi.org/10.1016/j.exco.2021.100025>.
- [16] A. JHA, *A residual based a posteriori error estimators for AFC schemes for convection-diffusion equations*, Computers & Mathematics with Applications, 97 (2021), pp. 86–99, <https://doi.org/10.1016/j.camwa.2021.05.031>.
- [17] A. JHA AND V. JOHN, *A study of solvers for nonlinear AFC discretizations of convection–diffusion equations*, Computers & Mathematics with Applications, 78 (2019), pp. 3117–3138, <https://doi.org/10.1016/j.camwa.2019.04.020>.
- [18] A. JHA AND V. JOHN, *On basic iteration schemes for nonlinear AFC discretizations*, in Lecture Notes in Computational Science and Engineering, Springer International Publishing, 2020, pp. 113–128, https://doi.org/10.1007/978-3-030-41800-7_7.
- [19] V. JOHN AND P. KNOBLOCH, *On spurious oscillations at layers diminishing (SOLD) methods for convection–diffusion equations: Part i – a review*, Computer Methods in Applied Mechanics and Engineering, 196 (2007), pp. 2197–2215, <https://doi.org/10.1016/j.cma.2006.11.013>.
- [20] V. JOHN AND P. KNOBLOCH, *On algebraically stabilized schemes for convection-diffusion-reaction problems*, 2021, <https://arxiv.org/abs/2111.08697>. submitted.
- [21] V. JOHN, J. MAUBACH, AND L. TOBISKA, *Nonconforming streamline-diffusion-finite-element-methods for convection-diffusion problems*, Numerische Mathematik, 78 (1997), pp. 165–188, <https://doi.org/10.1007/s002110050309>.
- [22] V. JOHN AND J. NOVO, *A robust SUPG norm a posteriori error estimator for stationary convection–diffusion equations*, Computer Methods in Applied Mechanics and Engineering, 255 (2013), pp. 289–305, <https://doi.org/10.1016/j.cma.2012.11.019>.
- [23] P. KNOBLOCH, *On the discrete maximum principle for algebraic flux correction schemes with limiters of upwind type*, in Lecture Notes in Computational Science and Engineering, Springer International Publishing, 2017, pp. 129–139, https://doi.org/10.1007/978-3-319-67202-1_10.
- [24] R. KORNUBER AND R. ROITZSCH, *On adaptive grid refinement in the presence of internal or boundary layers.*, Tech. Report SC-89-05, ZIB, Takustr. 7, 14195 Berlin, 1989.

- [25] D. KUZMIN, *Algebraic flux correction for finite element discretizations of coupled systems*, in Proceedings of the Int. Conf. on Computational Methods for Coupled Problems in Science and Engineering, M. Papadrakakis, E. Oñate, and B. Schrefler, eds., CIMNE, Barcelona, 2007, pp. 1–5.
- [26] M.-C. RIVARA, *Mesh refinement processes based on the generalized bisection of simplices*, SIAM Journal on Numerical Analysis, 21 (1984), pp. 604–613, <https://doi.org/10.1137/0721042>.
- [27] H. G. ROOS, M. STYNES, AND L. TOBISKA, *Robust numerical methods for singularly perturbed differential equations*, vol. 24 of Springer Series in Computational Mathematics, Springer-Verlag, Berlin, second ed., 2008. Convection-diffusion-reaction and flow problems.
- [28] U. WILBRANDT, C. BARTSCH, N. AHMED, N. ALIA, F. ANKER, L. BLANK, A. CAIAZZO, S. GANESAN, S. GIÈRE, G. MATTHIES, R. MEESALA, A. SHAMIM, J. VENKATESAN, AND V. JOHN, *Par-MooN—a modernized program package based on mapped finite elements*, Computers & Mathematics with Applications, 74 (2017), pp. 74–88, <https://doi.org/10.1016/j.camwa.2016.12.020>.